Shocked Silica Aerogel Radiance Transition

B. J. Henderson,[1,2] J. R. Rygg,[1,2,3] M. C. Marshall,[1] M. K. Ginnane,[1] L. E. Hansen,[4] E. Davies,[5] P. M. Celliers,[5] and G. W. Collins[1,2,3]

[1)] *Laboratory for Laser Energetics, University of Rochester, Rochester, New York 14623-1299, USA*

[2)] *Department of Physics and Astronomy, University of Rochester, Rochester, New York 14627, USA*

[3)] *Department of Mechanical Engineering, University of Rochester, Rochester, New York 14627, USA*

[4)] *Sandia National Laboratories, PO Box 5800, Albuquerque, New Mexico 87185-1189, USA*

[5)] *Lawrence Livermore National Laboratory, Livermore, California 94550, USA*

(Dated: 3 August 2022)

Silica (SiO_2) aerogel is widely used in high-energy-density shock experiments due to its low and adjustable density. Reported here are measurements of the shock velocity, optical radiance, and reflectivity of shocked SiO_2 aerogel with initial densities of 0.1, 0.2, and 0.3 g/cm^3. These results are compared with similar data from three solid polymorphs of SiO_2, silica, quartz, and stishovite with initial densities 2.2, 2.65, and 4.3 g/cm^3, respectively. Interestingly, below a brightness temperature of $T_{bright} \approx 35,000$ K, the slope of the radiance versus shock velocity is the same for each of the SiO_2 aerogels and solid polymorphs. At $T_{bright} \approx 35,000$ K, there is an abrupt change in the radiance versus shock velocity slope for aerogels, but not seen in the solid polymorphs over the pressures and temperatures explored here. An empirical model of shock front radiance as a function of SiO_2 density and laser drive parameters is reported to aid in design of experiments requiring maximum shock front radiance.

Keywords: High energy density physics (HEDP), shock, silica, aerogel, radiance

I. INTRODUCTION

SiO_2 aerogel has found many applications in high-pressure physics due to its microstructure and highly-deformable nature. Examples of SiO_2 aerogel's applications include laboratory astrophysics,[1,2] inertial confinement fusion (ICF) target design,[3] impedance matching standards[4–6] and complete equation-of-state (EOS) measurements,[7] radiative shocks,[8] additive foam targets,[9,10] and capture of high velocity (km/s) space particles.[11] Due to the collapse of its porous structure upon compression, aerogels can produce multi-eV (1 eV $\approx$ 11,600 K) temperatures using a relatively low pressure drive. As a well-characterized broadband source, shocked SiO_2 aerogel can probe optical absorption and reflectance during band structure changes[12–16] and ionization events[17–23] using spectrally-resolved optical diagnostics.[24,25]

The objective of this work was to measure the radiance of shock fronts in SiO_2 aerogel at various initial densities. The optical properties of shock compressed fused silica, quartz[26] and stishovite[27] have been characterized and used as standards for temperature and reflectance measurements.[28] This work measures the optical radiant behavior of shock compressed SiO_2 aerogel, which is expected to be significantly hotter and thus brighter at comparable shock pressures, than shock-compressed SiO_2 starting at solid density.[29,30] These measurements can be used to constrain radiative hydrodynamics in ICF simulations of implosions using aerogel liners, and to generate an optimally-bright broadband source for HEDP experiments.

The high-pressure behavior of shock compressed SiO_2 aerogel ($\rho_0 < 0.5$ g/cm^3) has been studied previously with efforts to understand its thermodynamic[31,32] and radiation transport properties.[33] Molecular dynamics simulations have been performed to show that macroscopic measurements of thermodynamic properties in shocked silica aerogel can be reproduced with nanoscale simulations.[34] Here we provide the first systematic radiance measurements of shock compressed SiO_2 aerogel, which when combined with shock wave data from several SiO_2 solid polymorphs, provides the radiant properties of shock-compressed SiO_2 with initial (and final) densities spanning more than an order of magnitude.

Laser-driven shocks were used to compress SiO_2 aerogel samples from initial densities of 0.1, 0.2, and 0.3 g/cm^3. Reflectivity, radiance, and shock velocity measurements from *in-situ* optical diagnostics are reported. Brightness temperature (T_{bright}) and pressure (P) are calculated through diagnostic calibration and Hugoniot measurements, respectively. A change in $T_{bright} - P$ behavior was detected near 35,000 K along the aerogel Hugoniot, and physical mechanisms (photoexcitation, electron/ion conduction, and microstructure) leading to this change are discussed. Finally, this dataset is leveraged for experimental design through an analytic model of shock-front radiance for a given laser drive irradiance.

In this work, the term "temperature" will be used in two distinctly different ways: (1) “temperature” by itself refers to the thermodynamic value derived from an EOS model and (2) “brightness temperature” refers to the value corresponding to a measured radiance centered at

600 nm. Finally, "radiance" refers to a measured photon flux per steradian (W/m^2sr) where an emissivity (ϵ) correction is not included ($\epsilon = 1$ representing a blackbody source).

II. EXPERIMENTAL TECHNIQUE

Experiments were performed on the OMEGA EP Laser System[35] at the University of Rochester's Laboratory for Laser Energetics. Targets were irradiated by one to four laser beams ($\lambda = 351$ nm) on a polystyrene (CH) ablator, producing strong shock waves that compress the planar samples.[36–40] These experiments used laser irradiance between 10 and 200 TW/cm^2 produced by 2-, 2.5-, and 4-ns temporally square and ramp-top laser pulses with spatially uniform spot diameters of approximately 1100 or 1800 μm through the use of distributed phase plates.

The targets (shown at the top of Fig. 1) are composed of a 40-μm CH ablator (refractive index $n = 1.59$ at $\lambda = 532$ nm, $\rho_0 = 1.05$ g/cm^3), a 50-μm quartz pusher ($n = 1.547$, $\rho_0 = 2.65$ g/cm^3), and a 250-μm SiO_2 aerogel sample ($n = 1.02$ to 1.06, $\rho_0 = 0.1$ to 0.3 g/cm^3). The quartz acts as a radiance and reflectance reference for the SiO_2 aerogel samples. Quartz's pressure, density, and particle velocity (P, ρ, u_p) along the Hugoniot have been experimentally measured to 12 TPa using diamond and aluminum standards.[41] Temperature and reflectance have been measured in the 0.5- to 5-eV range.[26–28] The CH and quartz act as a preheat radiation shield for the aerogel by absorbing >99.7% of the 2- to 5-keV x rays generated by laser ablation. A high-viscosity epoxy was used to edge-bond the aerogel to the pusher, preventing wicking into the central portion of the aerogel (region of interest), but inadvertently creating a vacuum gap with an average gap width of 20 μm. When the shock exits the pusher, the quartz expands into the vacuum region and piles up on the aerogel, reforming a shock. Measurements in the aerogel are taken after the radiance has reached a maximum, not at the quartz/aerogel interface, so the vacuum gap does not impact the reported data.

Shock velocity, reflectivity, and radiance are measured using using a velocity interferometer for any reflector (VISAR)[42] and a streaked optical pyrometer (SOP).[43,44] Streak images for VISAR and SOP are shown in Fig. 1. VISAR uses a 532-nm laser probe, which reflects off shock front, Doppler shifting the reflected probe. VISAR fringe position corresponds to the shock velocity and the amplitude corresponds to the shock front's reflectance. The probe enters through the back surface of the aerogel sample (Fig. 1). Velocity, reflectance, and brightness temperature (calculated from radiance) of the shock front for shot 34510 are shown in Fig. 1. For all drive irradiances used here, the shock in CH ($t = 0$ to 2 ns) is strongly absorbing at the VISAR probe wavelength, so limited measurements are performed in the ablator. A slowly decaying shock is observed in the quartz ($t = 2$ to 4 ns), with the reflectance increasing as the shock moves away from the ablation front. X rays from the ablation front photo-ionize material ahead of the shock, increasing the opacity experienced by the VISAR probe. Just before the shock breaks out from the quartz into the aerogel ($t = 4$ ns), the reflectance reference is established, where the measured reflectance matches the expected value.[28] A loss of reflectance just after breakout from the quartz corresponds to quartz expanding into the vacuum gap. The expanded quartz piles up on the aerogel, creating a ramp in the shock's velocity over ~0.5 ns. The shock then decays as it propagates through the aerogel ($t = 4.5$ to 13 ns).

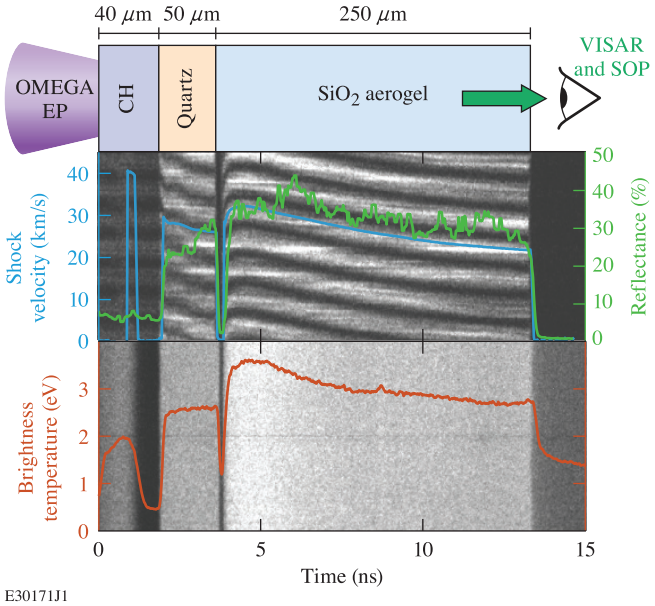

FIG. 1. (Top) Target setup used for these experiments. The CH is irradiated from the left side by the laser, driving a shock to the right. (Middle) Velocity (blue curve) and reflectance (green curve) extracted from shot 34510 over-plotted with the VISAR image. (Bottom) Brightness temperature (red curve, calculated from radiance) over-plotted with the SOP image.

III. ANALYSIS METHODS

Brightness temperature of the shocked aerogel was determined by measuring the radiance of the shock front using the SOP. SOP collects time- and spatially-resolved thermal emission from the shock front integrated over wavelengths between 590 and 850 nm, with a peak efficiency at 600 nm. The SOP signal is converted to brightness temperature using an absolute calibration of the OMEGA EP SOP, which follows the procedure described in Ref.[44]. Calculating brightness temperature requires an

assumption that light collected by the pyrometer is emitted from an optically thick surface located just behind shock front. Brightness temperature is calculated using the equation from Ref.[44]:

$$T_{bright} = \frac{T_0}{ln(1 + \frac{A_0}{\eta I})}, \quad (1)$$

where $T_0 = 1.990$ eV and $A_0 = 150,179$ ADU/ns are the OMEGA EP SOP calibration constants, η is the camera's sweep rate in pixels/ns, and I is the SOP counts in ADU/pixel. Analog-to-digital units (ADU's) have a 1:1 relationship with the number of CCD (charge-coupled device) electrons in a pixel. A systematic correction to the aerogel's radiance is calculated from the ratio of radiance measurements in the quartz reference and the expected radiance[28] at a given shock velocity. When fitting to the quartz radiance measurements, an uncertainty band is created which encompasses the shot-to-shot variations. This uncertainty band is projected onto the corrected aerogel brightness temperature, and added in quadrature with systematic uncertainties from the SOP calibration. Total uncertainty in the aerogel brightness temperature is quadrature sum of the random component (typical 2% uncertainty in the measured ADU's) and systematic components (3.5% uncertainty in A_0, 0.2% uncertainty in T_0,[44] 5-15% in T_{bright} from the quartz systematic correction). Uncertainty in the shock velocity is equal to $\sigma_{u_s} = 0.22$ km/s, or 5% of the velocity per fringe assigned to the interferometer's delay elements.

Reflectance is determined by comparing the VISAR fringe amplitude in the aerogel to that in the quartz. Average shock velocity, brightness temperature, and reflectance in aerogel for all shots included in the dataset are shown in Table I. SiO_2 aerogel follows a similar trend as quartz, where the reflectance drops significantly for shock velocities below 15 km/s. Uncertainty in the reflectance values are a quadrature sum of the random components (difference in measurement between the two VISAR systems and spatial variations in the measurement window) and systematic components (uncertainty in the quartz reflectance reference).

Brightness temperature versus inferred pressure data for all initial densities are shown in Fig. 2. For the aerogel measurements, pressure is inferred using an experimentally measured Hugoniot for 0.1 and 0.2 g/cm^3.[31] The Hugoniot for 0.3 g/cm^3 is approximated based on an assertion that for a given u_p, the u_s differs by 3% for each 0.1 g/cm^3 increment.[31,45] Parameters used for the aerogel $u_s - u_p$ curves are listed in Table II. Uncertainties in the 0.3-g/cm^3 Hugoniot are taken from the 0.2-g/cm^3 fit, with an increase of 50% to represent uncertainty in the approximation method. Inferred average EOS parameters for each shot are listed in Table III. Uncertainty in the inferred EOS parameters is on the order of 1.5%, 2%, 5%, and 5% of the reported particle velocity, pressure, density, and internal energy respectively; these are determined through a Monte Carlo routine that incorporates systematic uncertainties in the Hugoniots.

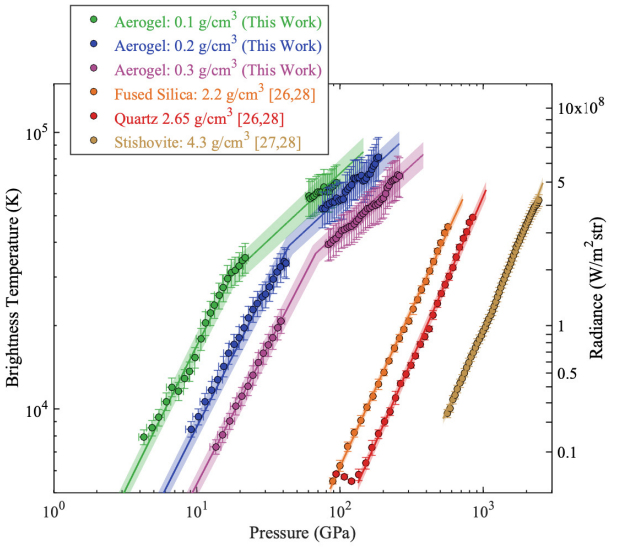

FIG. 2. Brightness temperature (and integrated radiance in the 590- to 850-nm band) versus inferred pressure for shock compressed SiO_2 aerogel (green, blue, and pink circles) and their two-part power-law fits (green, blue, and pink curves). Shaded regions represent 1-σ confidence intervals. Measurements on fused silica (orange circles),[26] quartz (red circles),[26] and stishovite (brown circles)[27] are fit with a single power-law function (orange, red, and brown curves).

Brightness temperature versus shock velocity data was fit with a bilinear function in log-log space in the form $log(T_{bright}) = a \cdot log(u_s) + log(b) - c \cdot \rho_0$, which is functionally equivalent to a two-part power law in the form $T_{bright} = b \cdot (u_s)^a \cdot e^{-c \cdot \rho_0}$ for linear-linear space. All three densities of aerogel are well represented by curves with identical a and b values, which change at the breakpoints located near $T_{bright} = 31$, 39, and 36 kK for 0.1, 0.2, and 0.3 g/cm^3, respectively. Breakpoint locations are determined by fitting the data above and below the gap in measurements and finding the intersection of the curves. The $c \cdot \rho_0$ term is a linear initial density correction on the curve's intercept. Below the breakpoint, c is the same value for all three curves. Above the breakpoint, c is the same for 0.2 and 0.3 g/cm^3 but differs by 2.5× for 0.1 g/cm^3. The parameters and 1-σ uncertainty (determined from the variance in the data) for the fits are shown in Table IV. The higher initial density polymorphs (fused silica, quartz,[26] and stishovite[27]) were fit with a single power law function, only including data points determined to be above melt.

SiO_2 aerogel exhibits behavior that is starkly different from its higher-density counterparts (Fig. 2). Specifically, the exponent of the power law a is ∼2 with no observed slope change for fused silica, quartz, and stishovite. For SiO_2 aerogel, a is 2 below the change in slope and ∼1 above the change in slope. Below the

change in slope observed in aerogel, the six $T_{bright} - P$ curves for SiO_2 form a set of parallel lines. Physical mechanisms leading to the anomalous brightness temperature behavior in aerogel are examined in Sec. V.

IV. RADIANCE MODEL

For the purpose of creating an optimally-bright SiO_2 photon source, an analytic shock-front radiance model was developed using a three-component target design composed of a CH ablator, quartz pusher, and SiO_2 sample. In this model the shock strength is assumed to be steady with time and optical absorption ahead of the shock is neglected. Ablation pressure is determined using a scaling law for CH ($\overline{Z} = 3.5$ and $\lambda_{laser} = 351$ nm):[46]

$$P_{ablation} = 346GPa \cdot \left(\frac{I_{laser}}{10^{13}}\right)^{2/3} \quad (2)$$

where I_{laser} is the maximum irradiance of the laser pulse in W/cm^2. For different laser wavelengths and ablator materials, the ablation pressure scaling law can be recalculated using the equation from Ref.[46]. The pressure and shock velocity in the SiO_2 sample is calculated using impedance matching[30] at the CH/quartz and quartz/SiO_2 interfaces. Experimentally determined Hugoniots for fused silica,[47] quartz,[5] stishovite,[27] 0.1- and 0.2-g/cm^3 aerogel[31] were used in the model. A Mie-Grüneisen linear reference[48] model was used for the quartz releasing into aerogel or fused silica. A reflected Hugoniot was used to model the reshock at both the quartz/stishovite and the CH/quartz interfaces. The brightness temperature in the SiO_2 sample is calculated using the inferred pressure from impedance matching and the two-part power-law fits. A Planck spectrum is calculated from the brightness temperature, and is integrated over the SOP's 590- to 850-nm band. The curves shown in Fig. 3 are the output of the radiance model. Uncertainty bands include the systematic uncertainty imposed during the impedance-matching process through the Hugoniot, release, and reshock models. Systematic uncertainties are incorporated through a Monte Carlo routine using $N = 10^6$ trials.

Since higher density SiO_2 polymorphs do not exhibit the same $T_{bright} - P$ slope change observed in aerogel, their shock front radiance curves will eventually overtake those of SiO_2 aerogel, as seen in Fig. 3. A photoexcitation-driven slope change is expected in higher density polymorphs of silica, however this would occur at pressures far exceeding (a few thousand GPa in fused silica and quartz) those sampled in this work. Thus, in order to obtain maximum brightness for a given fixed laser drive irradiance, aerogel should be selected as an emitter for laser drives below ~25 TW/cm^2. Additionally, fused silica is more effective than aerogel at coupling energy from the shock into pressure, due to its higher shock

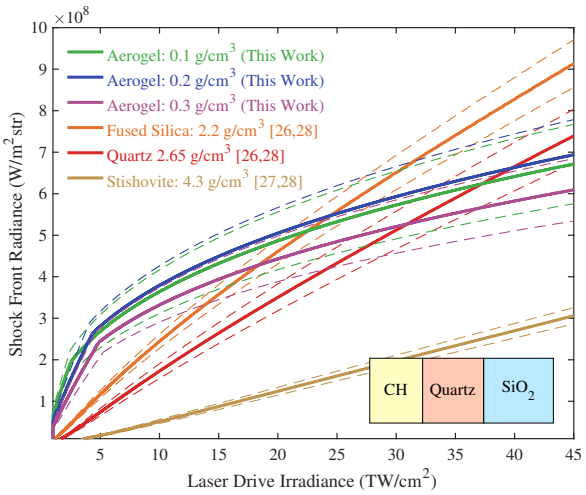

FIG. 3. Shock front radiance integrated over 590 to 850 nm versus laser drive irradiance for a three-component target design including: CH ablator, quartz pusher, and SiO_2 sample (inset). Aerogel targets produce the brightest shocks when driven with less than ~25 TW/cm^2. Dashed curves indicate a 1-σ confidence interval.

impedance. So, at higher laser drive irradiances, a larger fraction of the deposited laser energy will be converted into compression and shock fronts in fused silica will be brightest.

This model can be applied to a variety of different ablators, pushers, and samples. In the model results presented, the quartz is kept inside the target as radiation shielding from the laser drive. When designing a bright optical source, mitigating radiation flux from the ablation front may be needed to minimize the initial photoexcitation of the sample material, thus maximizing the shock's brightness. A 40-μm CH ablator and 50-μm quartz pusher reduce the number of 2- to 5-keV x rays from the ablation front by 99.7%. When designing a source with maximum brightness, maintaining radiation shielding of >99% will ensure that the radiance model is an accurate predictor for the experiment.

V. DISCUSSION

The change in slope exhibited by the brightness temperature in SiO_2 aerogel warrants further investigation. When compared against Thomas-Fermi[29] and density functional theory-based equations of state,[32] the EOS temperature and measured brightness temperature differ by 50% to 100%, with increasing disagreement at the highest shock velocities. This disagreement has been previously observed in Ta_2O_5 foams with an initial density of 0.25 g/cm^3.[49] Some possible causes for this difference include: (a) radiative precursor ahead of the shock, (b) a conductive precursor, and (c) shock propagation in aerogel microstructure.

Shock fronts with brightness temperatures in the eV range emit photons with energies high enough to stimulate electronic transitions in ambient material ahead of the shock. These multi-eV photons will increase the opacity ahead of the shock, decreasing the signal measured by SOP. Loss of reflectance at high shock velocities has been attributed to photoexcitation ahead of the shock.[50] SiO_2 aerogel might be more susceptible to photoexcitation than higher density polymorphs, but further constraints on the UV transmission of aerogel foams is needed to accurately estimate the optical absorption ahead of the shock.

A conductive precursor could be streaming ahead of the shock front in aerogels. The work of Ref.[32] simulated the diffusion of high temperature ions ahead of the shock and found that the ions are significantly slower than the shock front ($v_{diffusion} < 0.1u_s$). However, these simulations do not calculate electron diffusion ahead of the shock. Electrons ionized by the compression may diffuse into the ambient material at velocities faster than the shock front, increasing the free carrier density and opacity ahead of the shock. Measurements of electronic conductivity in SiO_2 aerogel at various densities are needed to accurately estimate the effects of free carrier diffusion ahead of the shock front.

The dynamics of shock propagation in highly-porous materials is significantly different from that of solid crystals.[30] X-ray radiography measurements of shocks in aerogels show that shock fronts disperse as they propagate through the microstructure.[51] An aerogel with ambient density of 0.1 to 0.3 g/cm^3 is 96 to 87% voids, respectively. Samples used in these experiments had pores smaller than 40 nm, significantly smaller than the resolution of VISAR and SOP ($\sim 10\mu m$). These diagnostics will not be able to detect spatial variations in the shock front due to the microstructure, but it may have an effect on the bulk measurements.

VI. CONCLUSIONS

In conclusion, shock velocity, radiance, reflectance, and inferred brightness temperature of shocks in SiO_2 aerogel were determined when singly shocked from 0.1, 0.2, and 0.3 g/cm^3. SiO_2 aerogel's brightness temperature versus pressure behavior was starkly different from higher density polymorphs. A change in slope of the brightness temperature versus pressure was detected in all three initial densities near 35,000 K, but is not seen in higher density polymorphs of SiO_2. The observed change in slope could be due to radiative, conductive, or microstructure effects. This observation is of fundamental importance for experiments using SiO_2 aerogel and strong shocks. Some of these applications include laboratory astrophysics,[1,2] ICF target designs with aerogel liners,[3] EOS measurements,[4–7] radiative shock experiments,[8] additive foam target designs,[9,10] and high-pressure optical property experiments.

Using measurements from six different initial densities of SiO_2, a radiance model was developed for pragmatic experimental design. These sources are of great interest for measurements of optical absorption and reflectance during band structure changes[12–16] and ionization events[17–23]. For the purpose of generating a broadband optical probe, SiO_2 aerogels are an optimally-bright source when using laser drivers below $\sim$25 TW/cm^2. At stronger drive irradiances, aerogel becomes less optimal due to the reduction in $T_{bright} - P$ slope.

AUTHOR'S CONTRIBUTIONS

All authors contributed equally to this work.

ACKNOWLEDGEMENTS

This material was based upon work supported by the Department of Energy National Nuclear Security Administration under Award No. DE-NA0003856, the University of Rochester, and the New York State Energy Research and Development Authority. A portion of this work was performed under the auspices of NSF Physics Frontier Center Award No. PHY-2020249, and under the auspices of the US Department of Energy by Lawrence Livermore National Laboratory under Contract No. DE-AC52-07NA27344. This report was prepared as an account of work sponsored by an agency of the US Government. Neither the US Government nor any agency thereof, nor any of their employees, makes any warranty, express or implied, or assumes any legal liability or responsibility for the accuracy, completeness, or usefulness of any information, apparatus, product, or process disclosed, or represents that its use would not infringe privately owned rights. Reference herein to any specific commercial product, process, or service by trade name, trademark, manufacturer, or otherwise does not necessarily constitute or imply its endorsement, recommendation, or favoring by the US Government or any agency thereof. The views and opinions of authors expressed herein do not necessarily state or reflect those of the US Government or any agency thereof.

DATA AVAILABILITY

The data that support the findings of this study are available from the corresponding author upon reasonable request.

[1] C. Liu, K. Matsuo, S. Ferri, H-. K. Chung, S. Lee, S. Sakata, K. F. F. Law, H. Morita, B. Pollock, J. Moody, and S. Fujioka, High Energy Density Physics **33**, 100710 (2019)

[2] H. Louis, A. Demiris, K. S. Budil, P. L. Miller, T. A. Peyser, D. A. Wojtowicz, and P. E. Dimotakis, J. Fusion Technol. **28**, 1833 (1995).

[3]S. W. Haan, M. C. Herrmann, P. A. Amendt, D. A. Callahan, T. R. Dittrich, M. J. Edwards, O. S. Jones, M. M. Marinak, D. H. Munro, S. M. Pollaine, J. D. Salmonson, B. K. Spears, and L. J. Suter, Fusion Sci. Technol. **49**, 553 2006.

[4]M. D. Knudson, J. R. Asay, and C. Deeney, J. Appl. Phys. **97**, 073514 (2005).

[5]M. D. Knudson and M. P. Desjarlais, Phys. Rev. Lett. **103**, 225501 (2009).

[6]M. C. Gregor, D. E. Fratanduono, C. A. McCoy, D. N. Polsin, A. Sorce, J. R. Rygg, G. W. Collins, T. Braun, P. M. Celliers, J. H. Eggert, D. D. Meyerhofer and T. R. Boehly, Phys. Rev. B **95**, 144114 (2017).

[7]K. Falk, L. A. Collins, E. J. Gamboa, G. Kagan, J. D. Kress, D. S. Montgomery, B. Srinivasan, P. Tzeferacos, and J. F. Benage, Phys. Plasmas **51**, 056309 (2014)

[8]T. E. Tierney IV, H. E. Tierney, G. C. Idzorek, R. G. Watt, R. R. Peterson, D. L. Peterson, C. L. Fryer, M. R. Lopez, M. C. Jones, D. Sinars, G. A. Rochau, and J. E. Bailey, Rev. Sci. Instrum. **79**, 10E919 (2008)

[9]S. Zhao, G. Siqueira, S. Drdova, D. Norris, C. Ubert, A. Bonnin, S. Galmarini, M. Ganobjak, Z. Pan, S. Brunner, G. Nyström, J. Wang, M. M. Koebel, and W. J. Malfait, Nature **584**, 387-393 (2020)

[10]K. B. Fournier, C. Constantin, J. Poco, M. C. Miller, C. A. Back, L. J. Suter, J. Satcher, J. Davis, and J. Grun, Phys. Rev. Lett. **92**, 16 (2004)

[11]D. Brownlee, P. Tsou, J. Aléon, C. M. Alexander, T. Araki, S. Bajt, G. A. Baratta, R. Bastien, P. Bland, P. Bleuet, *et al.*, Science **314**, 5806 (2006)

[12]Y. Ma, M. Eremets, A. R. Oganov, Y. Xie, I. Trojan, S. Medvedev, A. O. Lyakhov, M. Valle, and V. Prakapenka, Nature **458**, 182 (2009).

[13]M. Gatti, I. V. Tokatly, and A. Rubio, Phys. Rev. Lett. **104**, 216404 (2010).

[14]M. Marqués, M. Santoro, C. L. Guillaume, F. A. Gorelli, J. Contreras-García, R. T. Howie, A. F. Goncharov, and E. Gregoryanz, Phys. Rev. B **83**, 184106 (2011).

[15]D. N. Polsin, A. Lazicki, X. Gong, S. J. Burns, F. Coppari, L. E. Crandall, B. J. Henderson, K. Hilleke, M. F. Huff, M. I. McMahon, M. Millot, R. Paul, R. F. Smith, X. Wang, E. Zurek, J. H. Eggert, G. W. Collins, and J. R. Rygg, "Ramp-Compressed Sodium at 480 GPa: A Dense Electride," to be published in Nature Communications.

[16]N. W. Ashcroft, Nature **458**, 158 (2009).

[17]A. Ravasio, M. Bethkenhagen, J. A. Hernandez, A. Benuzzi-Mounaix, F. Datchi, M. French, M. Guarguaglini, F. Lefevre, S. Ninet, R. Redmer, and T. Vinci, Phys. Rev. Lett. **126**, 025003 (2021).

[18]E. Wigner and H. B. Huntington, J. Chem. Phys. **3**, 764 (1935).

[19]P. M. Celliers, G. W. Collins, L. B. Da Silva, D. M. Gold, R. Cauble, R. J. Wallace, M. E. Foord, and B. A. Hammel, Phys. Rev. Lett. **84**, 5564 (2000).

[20]M. Zaghoo and I. F. Silvera, Proc. Natl. Acad. Sci. **114**, 11873 (2017).

[21]R. P. Dias and I. F. Silvera, Science **355**, 715 (2017); **357**, eaao5843 (2017).

[22]M. Millot, S. Hamel, J. R. Rygg, P. M. Celliers, G. W. Collins, F. Coppari, D. E. Fratanduono, R. Jeanloz, D. C. Swift, and J. H. Eggert, Nat. Phys. **14**, 297 (2018).

[23]L. Crandall, J. R. Rygg, D. Spaulding, T. R. Boehly, S. Brygoo, P. M. Celliers, J. H. Eggert, D. E. Fratanduono, B. J. Henderson, M. F. Huff, R. Jeanloz, A. Lazicki, M. C. Marshall, D. N. Polsin, M. Zaghoo, M. Millot, and G. W. Collins, Phys. Rev. Lett. **125**, 165701 (2020).

[24]S. J. Ali, C. A. Bolme, G. W. Collins, and R. Jeanloz, Rev. Sci. Instrum. **86**, 043112 (2015).

[25]B. J. Henderson, M. Zaghoo, G. W. Collins, J. R. Rygg, and T. Boehly, Bull. Am. Phys. Soc. **63**, BAPS.2018.DPP.UO7.10 (2018).

[26]D. G. Hicks, T. R. Boehly, J. H. Eggert, J. E. Miller, P. M. Celliers, and G. W. Collins, Phys. Rev. Lett. **97**, 025502 (2006).

[27]M. Millot, N. Dubrovinskaia, A. Černok, S. Blaha, L. Dubrovinsky, D. G. Braun, P. M. Celliers, G. W. Collins, J. H. Eggert, and R. Jeanloz, Science **347**, 418 (2015).

[28]S. Brygoo, M. Millot, P. Loubeyre, A. E. Lazicki, S. Hamel, T. Qi, P. M. Celliers, F. Coppari, J. H. Eggert, D. E. Fratanduono, D. G. Hicks, J. R. Rygg, R. F. Smith, D. C. Swift, G. W. Collins, and R. Jeanloz, J. Appl. Phys. **118**, 195901 (2015).

[29]J. C. Boettger, Los Alamos National Laboratory NM, New Mexico, Report LA-11488-MS (1989).

[30]Ya. B. Zel'dovich and Yu. P. Raĭzer, *Physics of Shock Waves and High-Temperature Hydrodynamic Phenomena*, Vol. I (Academic Press, New York, 1966).

[31]M. D. Knudson and R. W. Lemke, J. Appl. Phys. **114**, 053510 (2013).

[32]K. Falk, C. A. McCoy, C. L. Fryer, C. W. Greeff, A. L. Hungerford, D. S. Montgomery, D. W. Schmidt, D. G. Sheppard, J. R. Williams, T. R. Boehly, and J. F. Benage, Phys. Rev. E **90**, 033107 (2014).

[33]K. Falk, D. Jung, N. Guler, O. Deppert, M. Devlin, J. C. Fernandez, D. C. Gautier, M. Geissel, R. C. Haight, B. M. Hegelich, D. Henzlova, K. D. Ianakiev, M. Iliev, R. P. Johnson, F. E. Merrill, G. Schaumann, K. Schoenberg, T. Shimada, T. N. Taddeucci, J. L. Tybo, F. Wagner, S. A. Wender, G. A. Wurden, A. Favalli, and M. Roth, Bull. Am. Phys. Soc. **59**, BAPS.2014.DPP.BO5.14 (2014).

[34]S. P. Patil, P. Shendye, and B. Markert, Materialia **6**, 100315 (2019)

[35]D. D. Meyerhofer, J. Bromage, C. Dorrer, J. H. Kelly, B. E. Kruschwitz, S. J. Loucks, R. L. McCrory, S. F. B. Morse, J. F. Myatt, P. M. Nilson, J. Qiao, T. C. Sangster, C. Stoeckl, L. J. Waxer, and J. D. Zuegel, J. Phys.: Conf. Ser. **244**, 032010 (2010).

[36]S. I. Anisimov, A. M. Prokhorov, and V. E. Fortov, Sov. Phys. Usp. **27**, 181 (1984).

[37]S. A. Abrosimov, A. P. Bazhulin, V. V. Voronov, A. A. Geras'kin, I. K. Krasyuk, P. P. Pashinin, A. Yu. Semenov, I. A. Stuchebryukhov, K. V. Khishchenko, and V. E. Fortov, Quantum Electron. **43**, 246 (2013).

[38]I. K. Krasyuk, P. P. Pashinin, A. Yu Semenov, K. V. Khishchenko, and V. E. Fortov, Laser Phys. **26**, 094001 (2016).

[39]G. W. Collins, L. B. Da Silva, P. Celliers, D. M. Gold, M. E. Foord, R. J. Wallace, A. Ng, S. V. Weber, K. S. Budil, and R. Cauble, Science **281**, 1178 (1998).

[40]R. Cauble, T. S. Perry, D. R. Bach, K. S. Budil, B. A. Hammel, G. W. Collins, D. M. Gold, J. Dunn, P. Celliers, L. B. Da Silva, M. E. Foord, R. J. Wallace, R. E. Stewart, and N. C. Woolsey, Phys. Rev. Lett. **80**, 1248 (1998).

[41]M. C. Marshall, A. E. Lazicki, D. Erskine, R. A. London, D. E. Fratanduono, P. M. Celliers, J. H. Eggert, F. Coppari, D. C. Swift, P. A. Sterne, H. D. Whitley, and J. Nilsen, Phys. Rev. B **99**, 174101 (2019).

[42]P. M. Celliers, D. K. Bradley, G. W. Collins, D. G. Hicks, T. R. Boehly, and W. J. Armstrong, Rev. Sci. Instrum. **75**, 4916 (2004).

[43]J. E. Miller, T. R. Boehly, A. Melchior, D. D. Meyerhofer, P. M. Celliers, J. H. Eggert, D. G. Hicks, C. M. Sorce, J. A. Oertel, and P. M. Emmel, Rev. Sci. Instrum. **78**, 034903 (2007).

[44]M. C. Gregor, R. Boni, A. Sorce, J. Kendrick, C. A. McCoy, D. N. Polsin, T. R. Boehly, P. M. Celliers, G. W. Collins, D. E. Fratanduono, J. H. Eggert, and M. Millot, Rev. Sci. Instrum. **87**, 114903 (2016).

[45]M. V. Zhernokletov, T. S. Lebedeva, A. B. Medvedev, M. A. Mochalov, A. N. Shuykin, and V. E. Fortov, AIP Conf. Proc. **620**, 763 (2002).

[46]R. P. Drake, *High-Energy-Density Physics: Fundamentals, Inertial Fusion, and Experimental Astrophysics*, Shock Wave and High Pressure Phenomena (Springer, Berlin, 2006).

[47]C. A. McCoy, M. C. Gregor, D. N. Polsin, D. E. Fratanduono, P. M. Celliers, T. R. Boehly, and D. D. Meyerhofer, J. Appl. Phys.

119, 215901 (2016).
[48] M. P. Desjarlais, M. D. Knudson, and K. R. Cochrane, J. Appl. Phys. **122**, 035903 (2017).
[49] J. E. Miller, Ph.D. thesis, University of Rochester, 2007.
[50] P. M. Celliers, T. R. Boehly, C. A. Thomas, H. F. Robey, S. A. MacLaren, H. -S. Park, M. B. Schneider, K. Widmann, G. W. Collins, and O. L. Landen, *Reflectivity loss in shock front velocimetry*, APS SCCM 2015, Tampa, FL, United States
[51] W. M. Howard, J. D. Molitoris, M. R. DeHaven, A. E. Gash, and J. H. Satcher, Lawrence Livermore National Laboratory, New Mexico, Report UCRL-JC-146894 (2002).

Shot Number	u_s (km/s)	σ_{u_s}	R (normalized)	σ_R	T_{bright} (K)	$\sigma_{T_{bright}}$
34506	7.53	0.14	0.03	0.01	9900	700
34509	9.29	0.14	0.14	0.03	11300	850
34512	8.93	0.14	0.09	0.03	12600	1000
34511	10.2	0.14	0.06	0.03	15800	1400
34505	12.6	0.14	0.04	0.01	26700	2900
34503	14.5	0.14	0.12	0.04	29600	3400
34507	22.1	0.14	0.22	0.10	45800	6300
34510	25.9	0.14	0.34	0.10	52200	7600
34501	23.9	0.22	0.26	0.05	56400	8500
34508	28.2	0.14	0.34	0.09	59000	9100
34504	28.7	0.14	0.34	0.08	61200	9600
34502	29.5	0.14	0.34	0.06	69600	11500

TABLE I. Average measured shock velocity, reflectance, calculated brightness temperature, and uncertainties for each shot included in the dataset, sorted by increasing brightness temperature. In this table, only a single average value is reported for each shot. In Fig. 2 the shot data is binned in shock velocity, with bin width equal to the uncertainty in the shock velocity measurement.

Density (g/cm^3)	C_0 (km/s)	S
0.1	-0.700 ± 0.258	1.23 ± 0.01
0.2	-0.389 ± 0.184	1.25 ± 0.01
0.3	-0.078 ± 0.276	1.26 ± 0.02

TABLE II. Linear Hugoniot coefficients for SiO_2 aerogel. The Hugoniot has functional form $u_s = S \cdot u_p + C_0$. The coefficients for 0.1 and 0.2 g/cm^3 are taken directly from Ref.[31], values for 0.3 g/cm^3 are inferred by approximation.

Shot Number	u_p (km/s)	P (GPa)	ρ_0 (g/cm^3)	ρ (g/cm^3)	η	E (MJ/kg)
34506	6.68	5.61	0.11	0.99	9.00	28.4
34509	7.41	21.2	0.30	1.48	4.95	42.5
34512	7.47	13.7	0.20	1.23	6.14	39.8
34511	8.80	9.93	0.11	0.84	7.61	51.1
34505	10.8	15.0	0.11	0.77	7.02	78.1
34503	11.9	34.5	0.20	1.13	5.65	102
34507	17.5	117	0.30	1.46	4.85	236
34510	20.6	162	0.30	1.45	4.84	326
34501	19.5	93.4	0.20	1.08	5.39	277
34508	22.4	191	0.30	1.45	4.84	383
34504	23.9	75.6	0.11	0.65	5.94	402
34502	24.0	143	0.20	1.06	5.32	424

TABLE III. Inferred average EOS parameters for each shot, sorted by increasing brightness temperature. Uncertainty in the inferred EOS parameters is on the order of 1.5%, 2%, 5%, and 5% of the reported particle velocity (u_p), pressure (P), density (ρ), and internal energy (E), respectively. $\eta = \rho/\rho_0$ is the average compression ratio for each shot.

Region	a	b (K$\cdot\frac{km}{s}^{-a}$)	c (cm^3/g)
Below Breakpoint	2 ± 0.03	185 ± 16.0	1.2 ± 0.02
Above Breakpoint	0.95 ± 0.02	$3.28 \cdot 10^3$ ± 260	0.90* ± 0.02

TABLE IV. Two-part power-law fits applied to the SiO_2 aerogel brightness temperature and shock velocity data. These fits are of the form $T_{bright} = b \cdot (u_s)^a \cdot e^{-c \cdot \rho_0}$ and are valid for shocks in SiO_2 aerogel traveling between approximately 7.5 to 30 km/s. The breakpoint in the fit occurs at $T_{bright} = 31$, 39, and 36 kK for 0.1, 0.2, and 0.3 g/cm^3, respectively. (*) For 0.1 g/cm^3, $c = 2.25$ cm^3/g above the breakpoint.